



IFM – The Department of Physics, Chemistry and Biology

TFYA 20
Surface Physics

**Scanning Tunneling
Microscopy**

Page	Content
3-11	STM
3	Introduction
3-7	Operating principles
7-11	Physical basis of STM

SCANNING TUNNELING MICROSCOPY

1 INTRODUCTION

Before the invention of the scanning tunneling microscope (STM) in the early 1980's, the possibilities to study the atomic structure of surfaces were mainly limited to diffraction techniques using beams of x-rays, electrons, ions and other particles. Although very accurate surface-structure determinations can be made using these techniques, they have a spatially averaging character, providing little or no information on surface defects. With the field ion microscope, developed in the 1950's, the geometrical arrangement of atoms on the surface of sharply pointed tips can be resolved in real space, but the requirements on sample geometry and stability under the high electric fields used in the imaging process make the technique unsuitable for general-purpose microscopy. Also the transmission electron microscopy has the capability to resolve individual atoms, or at least individual row of atoms, but the applicability for surface studies is limited. Moreover, all the above-mentioned techniques are further restricted by requiring vacuum for their operation.

A breakthrough came when Binnig and Rohrer designed the first operating STM.¹ This instrument showed atomic-scale resolution with a capability to use many kinds of samples in many different environments (*e.g.* vacuum, air, and liquids). Binnig and Rohrer were awarded the 1986 Nobel prize for their achievement.

2 OPERATION PRINCIPLES OF THE STM

The central part of the STM is a sharp conductive tip which is moved in a very precise and controlled manner in three dimensions across the surface of the sample, as shown in Fig. 2.1. A small voltage is applied between tip and sample (typically a few mV to a few V, depending on the sample material) and when the tip is brought close enough to the sample (5-10 Å) a tunneling current flows (10 pA-10 nA). This is purely quantum mechanical phenomenon (classically there would be no current, since the region between tip and sample is insulating) as, as will be shown below, the current is exponentially dependent on the distance between tip and sample, varying approximately one order of magnitude per Ångström. By keeping the current constant, the distance to the sample is held constant and if the tip is scanned over the surface and its movement perpendicular to the sample required to keep the current constant is registered, the result is a topographical image of the sample surface. Alternatively, the tip is scanned across the sample surface at a constant average height and the current variations are registered (this requires a surface that does not contain large protrusion into which the tip would crash). As will be discussed below, the constant-current image is actually not a true topographical image but an image of the surface electron density that, for certain sample materials like metals, agrees fairly well with the true topography. The vertical resolution is limited by the mechanical stability of the instrument and the capability of the electronics to keep the current constant, something that is facilitated by the exponential dependence on the distance between tip and sample. Vertical resolution in the 0.01 Å range are readily accomplished. Horizontally, the resolution is limited by the sharpness of the tip, and 10 Å resolution is routinely achieved. Under favourable conditions a lateral resolution as high as 1 Å may be achieved, such that individual atoms can be resolved.

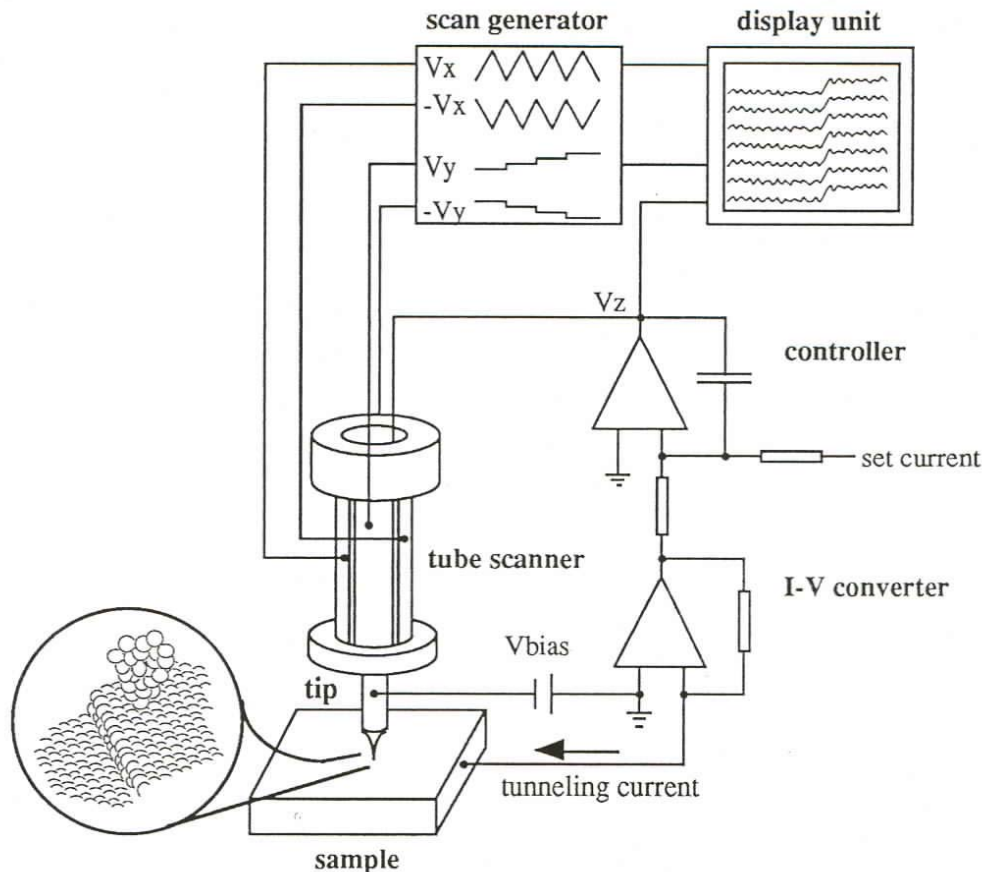


Fig. 2.1 Schematic picture of an STM with peripherals.

One of the advantages of STM is the possibility to use most kinds of sample materials, the only criterion being that the sample has to be conductive. STM has been used for determination of the surface structure of metals² and semiconductors³ as well as for studies of nucleation and growth of thin films in vacuum.⁴ Other applications include studies of biological materials⁵ and *in situ* studies of electrochemical reactions.⁶

There are applications of the STM other than pure topographical measurements, *e.g.* tunneling spectroscopy where different electronic states of the surface may be mapped with very high spatial resolution.³ Also emission of secondary particles such as electrons and photons induced by electrons from the tunneling tip have been studied with high spatial resolution using STM.⁷

Since the invention of the STM new exciting scanning probe techniques using different probe-sample interactions to control the separation have appeared. The most notable is the atomic force microscope⁸ (AFM) where the force between the tip and the sample is used in the same manner as the tunneling current in the STM. The resolution of the AFM is almost in the range of the STM and the sample materials do not have to be conductive.

2.1 Mechanical considerations

Due to the extremely small distances involved, the mechanical rigidity and vibration isolation are of utmost importance. From the first comparably voluminous STMs which required several stages of vibration isolation, the development has gone towards small and rigid microscopes with little or no vibration isolation at all.⁹ It has even been possible to fabricate working miniature STMs on silicon wafers.¹⁰

2.2 Positioning system

In an STM, two functions of the positioning system are required. Besides the need for a three-dimensional fine-positioning device to move the tip in the Ångström to micrometer range, a mechanism is needed to bring the tip and sample within the range of the fine-positioning device from millimeters apart.

The fine-positioning system has since the first STM been realized with piezo-electric ceramics. A piezo-electric material is a material that deforms in a controlled manner when a voltage is applied across it, with a typical sensitivity in the range of 10-100 Å/V. Basically two types of scanners are used, the tripod and the tube, see Fig. 2.2.

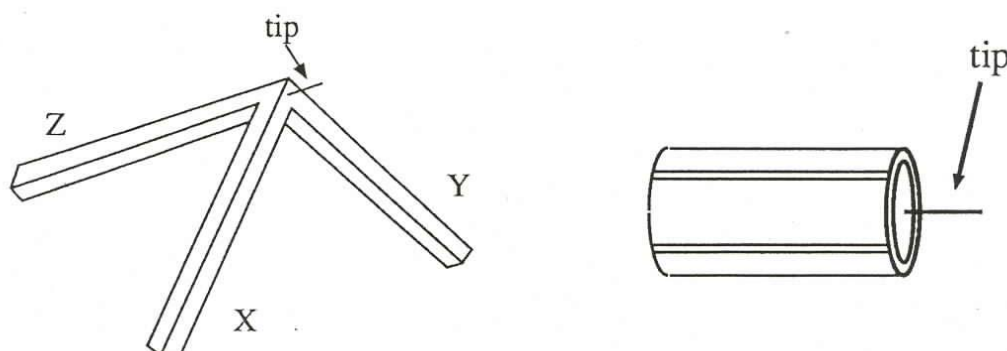


Fig. 2.2. Tripod scanner (left) and tube scanner (right).

The tripod scanner consists of three piezo rods orthogonally connected to each other to give a three-dimensional motion. The tube scanner consists of a single piezo-electric tube with one inner electrode and four axial and orthogonal electrodes. The z motion is a function of the voltage applied between the inner electrode and the outer electrodes and the lateral motion is achieved by applying a voltage between the inner and only one of the outer electrodes. This causes that particular segment to stretch or contract and the tube bends accordingly. Compared to the tripod, the tube scanner is more rigid and thus has a higher mechanical resonance frequency, making it possible to scan at a higher speed. Nowadays the tube scanner is the most common type of scanner.

A great variety of coarse-positioning devices have been presented and a simple example is to use a screw with some kind of gear. Another type is utilizing the inertia of a moving object as in the instrument used in this exercise. The sample holder consists of a circular metal plate with a hole in the centre where the sample, clamped to the upper face, is exposed to the tip coming up from below, *cf.* appendix. Parallel to the piezo-electric tube for the movement of the tip are three tubes also made of a piezo electric material. By applying appropriate voltages to the supporting tubes, the

sample holder may be rotated. This rotation is of course very small. However, if the driving voltages are applied in a sequence of slow rotations in one direction alternated by fast rotations in the opposite direction, the inertia of the sample holder will prevent it from moving during the fast part of the sequence resulting in a net rotation. If the procedure is repeated at a high frequency, the net motion is fast enough to be useful for the coarse approach.

2.5 Electronics

The most common imaging mode is the constant current mode, which requires a regulator that adjust the z driving voltage to keep the tunneling current at a preset value, as shown in the block diagram in Fig. 2.3.

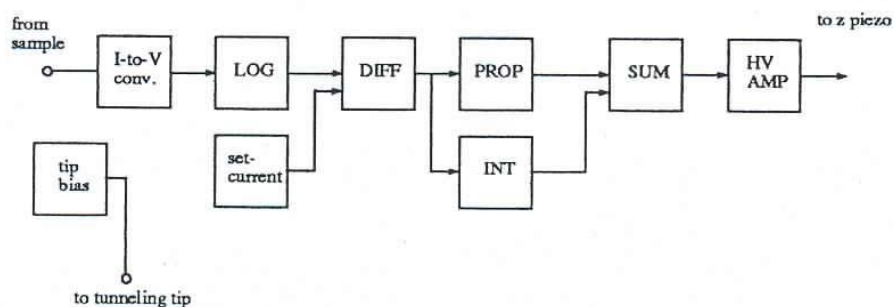


Fig. 2.3. The basic controller for the tunneling current.

The current from the sample is fed to a current-to-voltage converter whose output voltage is fed to a logarithmic amplifier that compensates for the exponential behavior of the tunneling junction. The signal is compared to the set current in a difference amplifier and the error signal is amplified in a proportional and sometimes also in an integrating stage. Finally, the signal is fed to the high voltage amplifier that drives the piezo element for the vertical motion of the tip, thus closing the feedback loop such that, *e.g.*, a too high current causes a retraction of the tip.

2.4 Tip

The performance of the STM is much dependent on the condition of the tip as it determines the resolution of the instrument. The tip consists of a mechanically or electro-chemically sharpened wire of *e.g.* tungsten, gold, or platinum. Ideally it has a monoatomic point, but the apex continuously rearranges and sample atoms adsorb during operation. Since the image actually is a convolution of the tip and the sample, the symmetry of the tip is reflected in the recorded image and several different tips must be used for a given sample before conclusions can be drawn about the surface structure. Sometimes tunneling current flows simultaneously from several parts of the tip and the resulting image is a superposition of more than one image. The problem with a blunt, double tip is illustrated in Fig. 2.4, where it can be seen that scanning the single protrusion on the sample with the double tip results in an image showing two “bumps”. When scanning with the sharp tip, the only distortion of the image is a slight broadening of the “bump”.

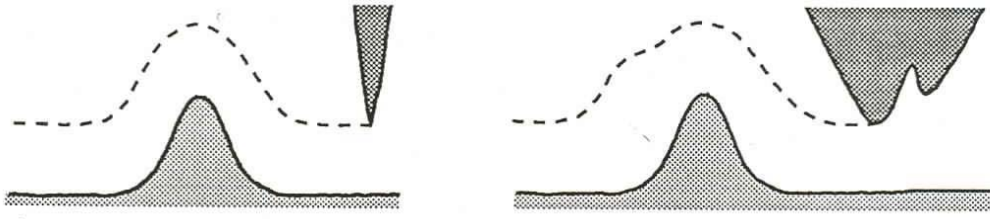


Fig. 2.4. The paths followed by a sharp tip (left) and a blunt, double tip (right)

3 PHYSICAL BASIS OF THE STM

A full treatment of the tunneling between tip and sample in an STM requires three-dimensional tunneling theory, well beyond the scope of this text. Instead, a one-dimensional treatment is presented, which gives results in qualitative agreement with three-dimensional theory.

A simple approach when modeling tunneling in one dimension is to assume that only elastic tunneling occurs, that the two (metallic) electrodes are semi-infinite potential wells with depth $E_F + \phi$, each as in Fig. 3.1.

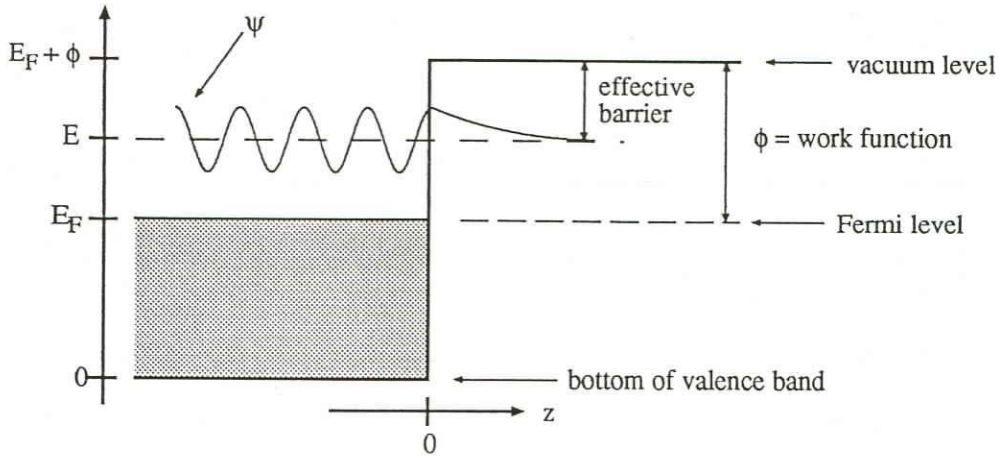


Fig. 3.1. Potential well with depth $E_F + \phi$ for modeling of a tunneling electrode.

The Schrödinger equation for one of the metal electrodes can be written as:

$$-\frac{\hbar^2}{2m} \frac{\partial^2}{\partial z^2} \psi(z) + V(z)\psi(z) = E\psi(z) \quad (3.1)$$

with the potential given by

$$V(z) = \begin{cases} 0, & z < 0 \\ E_F + \phi, & z \geq 0 \end{cases} \quad (3.2)$$

Inside the metal, $z < 0$: $V(z) = 0$, the Schrödinger equation is rewritten as:

$$-\frac{\hbar^2}{2m} \frac{\partial^2}{\partial z^2} \psi(z) = E\psi(z) \quad (3.3)$$

To solve this, a plane-wave solution is assumed, $\psi(z) = Ae^{ikz} + Be^{-ikz}$, which inserted into (3.3) gives:

$$-\frac{\hbar^2}{2m} \frac{\partial^2}{\partial z^2} (Ae^{ikz} + Be^{-ikz}) = E(Ae^{ikz} + Be^{-ikz}) \quad (3.4)$$

$$\Rightarrow k(E) = \sqrt{\frac{2mE}{\hbar^2}} \quad (3.5)$$

Outside the metal, $z \geq 0$: $V(z) = E_F + \phi$, the Schrödinger equation is rewritten as:

$$-\frac{\hbar^2}{2m} \frac{\partial^2}{\partial z^2} \psi(z) + (E_F + \phi)\psi(z) = E\psi(z) \quad (3.6)$$

Since the wave function must approach zero far away from the metal, a solution, a solution with exponential decay is assumed, $\psi(z) = Ce^{-\kappa z}$, which inserted into (3.6) gives:

$$-\frac{\hbar^2}{2m} C\kappa^2 e^{-\kappa z} = (E - (E_F + \phi))Ce^{-\kappa z} \quad (3.7)$$

$$\Rightarrow \kappa(E) = \sqrt{\frac{2m}{\hbar^2} ((E_F + \phi) - E)}, \quad (3.8)$$

where κ is the so-called inverse decay length and $((E_F + \phi) - E)$ is the effective barrier height, see Fig. 3.1.

To obtain the full solution of the Schrödinger equation (3.1) for the assumed potential (3.2), the above solutions for $z < 0$ and $z \geq 0$ must be matched at the interface by adjusting the coefficients A, B, and C such that the wave function and its derivative are continuous at $z = 0$. This yields a wave function that is periodic inside the metal and exponentially decaying outside.

To get a numeric value for the inverse decay length κ , we let $E = E_F$ and $\phi = 4.5$ eV, a typical value for a metal. This yields:

$$\kappa(E) = \sqrt{\frac{2m}{\hbar^2} ((E_F + \phi) - E)} = \sqrt{\frac{2m\phi}{\hbar^2}} \approx 1.1 \text{Å}^{-1} \quad (3.9)$$

The probability to find an electron with energy E at location Z is given by the probability distribution:

$$\rho(E, z) = \psi(E, z) * \psi(E, z) \quad (3.10)$$

and outside the electrode we get:

$$\rho(E, z) \sim e^{-2\kappa(E)z} \quad (3.11)$$

From this, we can see that:

- The probability distribution, ρ , decays roughly one order of magnitude when z is increased 1 \AA .
- Lower energy means larger κ , which implies a more rapid decay.

For a real metal with a more complex potential $V(z)$ and a density of states $g(E)$, the total probability of finding an electron with energy E at location z is given by the probability distribution (3.11) weighted by the density of states, and the situation may look like Fig. 3.2.

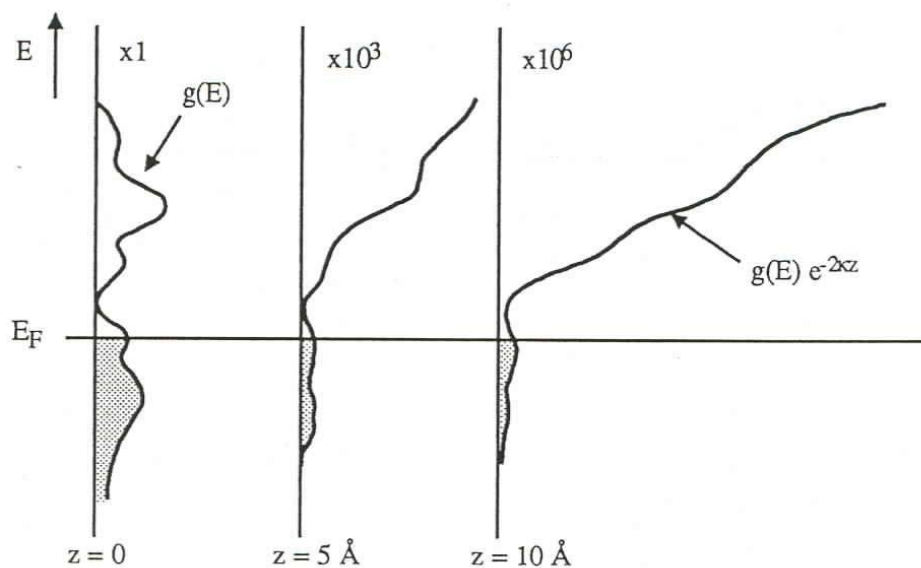


Fig. 3.2. The probability distribution ρ weighted by the density of states.

Two planar electrodes (modeled as potential-wells as described above) brought close to each other may be seen as an STM with an extremely blunt tip. This is depicted in Fig. 3.3 for a negative bias on the tip, *i.e.* the electrons tunnel from the tip to the sample.

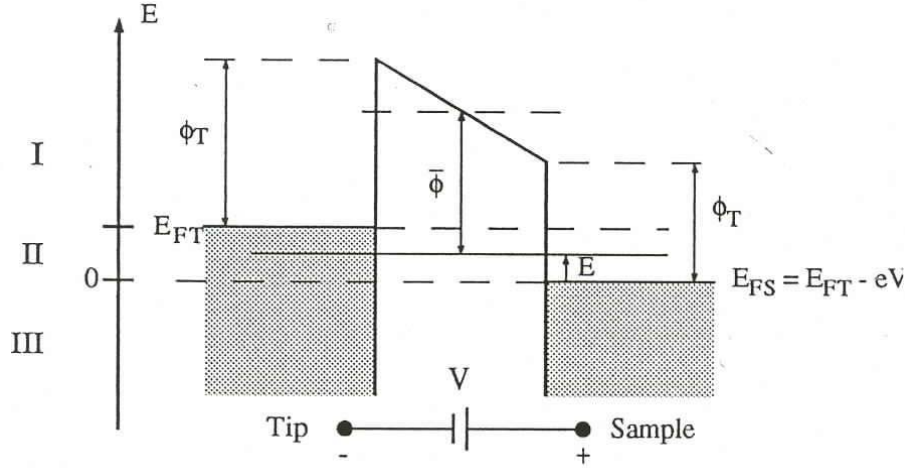


Fig. 3.3. Two potential wells brought close to each other which may be regarded as a one dimensional STM.

On the tip side there are no electrons that can contribute to a tunneling current for energies above the Fermi level, E_{FT} (region I in Fig. 3.3). For the region below the Fermi level of the sample, E_{FS} , (region III) electrons are available for tunneling on both sides of the junction but the net contribution to the tunneling is zero due to the fact that the tunneling probability is equal in both directions. Therefore the net tunneling current comes from the region between E_{FT} and E_{FS} (region II). As can be seen in Fig. 3.3, these electrons experience an average barrier height given by:

$$\bar{\phi} = \frac{\phi_T + \phi_S}{2} + \frac{eV}{2} - E \quad (3.12)$$

resulting in an inverse decay length equal to:

$$\kappa(E) = \sqrt{\frac{2m\bar{\phi}}{\hbar^2}} \quad (3.13)$$

We can now express the net tunneling current as given by the overlap between the wave functions of tip and sample weighted by the corresponding density of states:

$$I(V) \sim \int_{E_{FT}}^{E_{FS}} g_T(E) e^{-\kappa(E)r} g_S(E - eV) e^{-\kappa(E)s} dE \quad (3.14)$$

If we assume that these principles also hold for real samples and sharper tips, *i.e.* a smaller probe area and thus an increased lateral resolution, we obtain an expression for the tunneling current in the STM:

$$I(\vec{r}, V) \sim \int_0^{eV} g_T(\vec{r}, E) g_S(\vec{r}, E - eV) e^{-2\kappa(E)s} dE \quad (3.15)$$

Although several simplifying assumptions have been made in the derivation of this equation, the qualitative features are in agreement with results from more elaborate three-dimensional calculations.¹² The exponential dependence of the current on the tip-sample separation is evident from the equation. Moreover, it is seen that the tip and the sample are equivalent in the theory, and that the tunneling current is proportional to the convolution of the density of states. Ideally one would like to relate the STM image directly to the properties of the sample, which would require an ideal, infinitesimal tip with a constant density of states. This is not possible to achieve in practice, so the properties of the tip must always be taken into account when interpreting STM images. Even for an ideal tip, a constant-current STM image is not a true image of the topography of the sample surface, but rather a map of the surface electronic states.

REFERENCES

1. G. Binnig, H. Rohrer, Ch. Gerber, H. Weibel, *Phys. Rev. Lett.* **49**, 57 (1982)
2. R.J. Behm, in “Scanning Tunneling Microscopy and Related Methods”, R.J. Behm, N. Garcia, and H. Rohrer eds. (NATO ASI Series, Series E: Applied Sciences – vol.184)
3. R.M. Feenstra, in “Scanning Tunneling Microscopy and Related Methods”, R.J. Behm, N. Garcia, and H. Rohrer eds. (NATO ASI Series, Series E: Applied Sciences – vol.184)
4. H. Neddemeyer, *Critical Reviews in Solid State and Material Sciences* **16**, 309 (1990)
5. P.K. Hansma, V.B. Elings, O. Marti, and C.E. Bracker, *Science* **242**, 209 (1988)
6. H. Siegenthaler and R. Christoph, in “Scanning Tunneling Microscopy and Related Methods”, R.J. Behm, N. Garcia, and H. Rohrer eds. (NATO ASI Series, Series E: Applied Sciences – vol.184)
7. D.L. Abraham, A. Veider, Ch. Schönenberger, H.P. Meier, D.J. Arent, and S.F. Alvarado, *Appl. Phys. Lett.* **56**, 1564 (1990)
8. D. Rugar, and P. Hansma, *Physics Today* **43**, 23 (1990)
9. J.W. Lyding, S. Skala, J.S. Hubacek, R. Brockenbrough and G. Gammie, *Rev. Sci. Instrum.* **59**, 1897 (1988)
10. T.R. Albrecht, S. Akamine, M.J. Zdeblick, C.F. Quate, *J. Vac. Sci. Technol.* **A8** (1), 317 (1990)
11. Y. Kuk and P.J. Silverman, *Appl. Phys. Lett.* **48**, 1597 (1986)
12. J. Tersoff, in “Scanning Tunneling Microscopy and Related Methods”, R.J. Behm, N. Garcia, and H. Rohrer eds. (NATO ASI Series, Series E: Applied Sciences – vol.184)